Stability Analysis of Salt Fingers for Different Non-uniform Temperature Profiles in a Micropolar Liquid

Nisha Mary Daniel, Vennela Lingamneni, Tessy Tom, and N. Arun Kumar

1 Introduction

When heat is supplied to the fluid from above, the temperature makes the fluid molecules lighter at the upper layer, and hence it stabilizes the system. But, when we supply solute from above, the concentration of the solute molecules slowly enters the system and settles at the bottom, and due to this movement, the system becomes unstable and hence the concentration of solute destabilizes the system. In this case, we can observe that temperature stabilizes the system and the concentration destabilizes the system. The double diffusive instability induced by this case in literature is known as salt fingers. Double diffusive convection is a fluid dynamics phenomenon that occurs due to the difference in diffusivity rates of two different density gradients in the fluid. The difference in the thermal and salt diffusivity rates gives rise to instabilities called "salt fingers". Stern [1], Jevons [2], Ekman [3], and Stommel et al. [4] were among the first to explain the physical mechanism of double diffusive convection. Instability at the interface between a layer of denser fluid and an underlying layer of temperature stratified water was observed. Later researches verified that salt fingers develop at the thin interface where two layers of the fluid with constant concentrations of its two distinct density gradients, with different molecular diffusivities, meet. In nature, double diffusive convection is more often observed in large water bodies like seas and oceans. Other occurrences in nature include convection in molten-rock

N. Mary Daniel (✉)
Research Scholar, Department of Mathematics, CHRIST(Deemed to be University), Bengaluru, India
e-mail: nisha.daniel@res.christuniversity.in

V. Lingamneni
Department of Mathematics, Sir MV PU College, Karnataka, India

T. Tom
Department of Commerce and Management, CHRIST(Deemed to be University), Lavasa, India

N. Arun Kumar
School of Engineering and Technology, CHRIST(Deemed to be University), Bengaluru, India

chambers and sea-wind formations [4]. The study of this convection has found its way into many researches due to its wide range of applications in nature and industry.
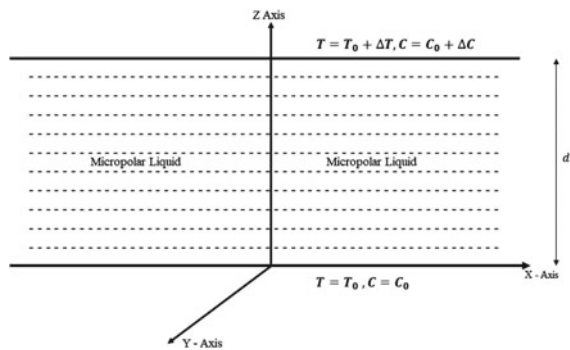
First introduced by Eringen [5], micropolar fluid theory establishes a class of fluids which demonstrates microrotational effects and can sustain body couples. In terms of its physical aspect, micropolar fluids comprise arbitrarily oriented rigid particles which can deform and rotate independently of the motion of the fluid, where the deformation of the particles is not considered. Micropolar fluids can model anisotropic fluids, liquid crystals with inflexible molecules, magnetic fluids, dusty clouds, muddy fluids, and a few biological fluids [5]. The theory of micropolar fluids is discussed in detail in the books of Eringen [5] and Lukasazewicz [6].

The goal of this paper is to investigate the stability of the system on the onset of salt finger convection under the influence of different non-uniform temperature profiles and to analyze the effect of certain micropolar parameters.

2   Mathematical Formulation

A layer of Boussinesquian micropolar liquid is considered between two horizontal plates of infinite length. These plates are kept at a distance "d" as shown in Fig. 1. Let T_0, C_0, and T, C be the temperature and solute concentration of the fluid at the lower and upper plates, respectively. Also, ΔT and ΔC be the temperature and solute concentration deviation of the fluid between the lower and upper plates. Suitable transport equations for both temperature and solute concentration are chosen considering effective heat capacity ratio and effective thermal diffusivity. The diagrammatic representation is examined under a Cartesian coordinate system where the origin and the x-axis coincide with the lower boundary and the z-axis is vertically upward [7]. Given below are the governing equations for the Boussinesquian micropolar liquid under double diffusive convection:

Fig. 1 Schematic diagram

$$\nabla.\mathbf{q} = 0, \tag{1}$$

$$\rho_0 \left[\frac{\partial \mathbf{q}}{\partial t} + (\mathbf{q}.\nabla)\mathbf{q} \right] = -\nabla p - \rho g \hat{k} + (2\xi + \eta)\nabla^2 \mathbf{q} + \xi \nabla \times \boldsymbol{\omega}, \tag{2}$$

$$\rho_0 I \left[\frac{\partial \boldsymbol{\omega}}{\partial t} + (\mathbf{q}.\nabla)\boldsymbol{\omega} \right] = (\lambda + \eta)\nabla(\nabla.\boldsymbol{\omega}) + \eta\nabla^2 \boldsymbol{\omega} + \xi(\nabla \times \mathbf{q} - 2\boldsymbol{\omega}), \tag{3}$$

$$\left[\frac{\partial T}{\partial t} + (\mathbf{q}.\nabla)T \right] = \chi\nabla^2 T + \frac{\beta}{\rho_0 C_v}(\nabla \times \boldsymbol{\omega}).\nabla T, \tag{4}$$

$$\rho = \rho_0[1 - \alpha_t(T - T_0) + \alpha_s(C - C_0)], \tag{5}$$

$$\left[\frac{\partial C}{\partial t} + (\mathbf{q}.\nabla)C \right] = \chi_s\nabla^2 C. \tag{6}$$

Here, q, ω, and p are the velocity, angular velocity, and pressure, respectively. ρ is the density of the liquid at temperature T and ρ_0 is the density at temperature T_0. g and I are the acceleration due to gravity and moment of inertia, respectively. ξ is the coefficient of coupling viscosity, λ, η, and λ', η' are the coefficients of bulk and shear spin viscosity, χ and χ_s are the thermal and solute conductivity, β is the coefficient of micropolar heat conduction, α_t and α_s are the coefficients of thermal and solutal expansion, respectively, σ is the electrical conductivity, and C_v is the specific heat at a constant volume.

3 Basic State

The basic state of the liquid in its quiescent condition is depicted by

$$\mathbf{q} = \mathbf{q}_b = (0, 0, 0), \, \boldsymbol{\omega} = \boldsymbol{\omega}_b = (0, 0, 0), \, p = p_b(z) = \rho = \rho_b(z), \tag{7}$$

$$\frac{dT_b}{dz} = \frac{\nabla T}{d}f(z), \, \frac{dC_b}{dz} = \frac{\nabla C}{d}g(z), \tag{8}$$

where the subscript "b" denotes the basic state. The basic temperature gradient $f(z)$ and concentration gradient $g(z)$ are non-dimensional and non-negative and satisfy the condition $\int_{d=0}^{d=1} f(z)\,dz$ and $\int_{d=0}^{d=1} g(z)\,dz$, respectively. The concerned basic state variable satisfies Eqs. (1) and (3) equivalently. This paper considers four different temperature profiles to analyze the onset of convection which is given below in Table 1.

4 Linear Stability Analysis

To examine the instability, an infinitesimal thermal perturbation is now introduced to the quiescent basic state of the liquid. We now have

Table 1 Non-uniform basic temperature profiles

S.No.	Profile	$f(z)$
CM1	Linear	$f(z) = 1$
CM2	Piecewise linear	$f(z) = \frac{1}{\epsilon} \qquad \forall\ 0 \leq z \leq \epsilon$ $\qquad\ \ 0 \qquad \forall\ \epsilon \leq z \leq 1$
CM3	Inverted parabolic	$f(z) = 2(1 - z)$
CM4	Parabolic	$f(z) = 2z$

$$\mathbf{q} = \mathbf{q}_b + \mathbf{q}', \boldsymbol{\omega} = \boldsymbol{\omega}_b + \boldsymbol{\omega}', \rho = \rho_b + \rho', p = p_b + p', \tag{9}$$

$$T = T_b + T', C = C_b + C'. \tag{10}$$

The subscript "b" indicates the basic state of the quantity and the primes denote the infinitesimal perturbations. By substituting Eq. (9) and (10) in Eqs. (1)–(6), we get the following linearized governing equations with respect to the infinitesimal perturbations:

$$\nabla.\mathbf{q}' = 0, \tag{11}$$

$$\rho_0 \left[\frac{\partial \mathbf{q}'}{\partial t} + (\mathbf{q}'.\nabla)\mathbf{q}' \right] = -\nabla p' - \rho' g\hat{k} + (2\xi + \eta)\nabla^2 \mathbf{q}' + \xi \nabla \times \boldsymbol{\omega}', \tag{12}$$

$$\rho_0 I \left[\frac{\partial \boldsymbol{\omega}'}{\partial t} + (\mathbf{q}'.\nabla)\boldsymbol{\omega}' \right] = (\lambda' + \eta')\nabla(\nabla.\boldsymbol{\omega}') + \eta'\nabla^2 \boldsymbol{\omega}' + \xi(\nabla \times \mathbf{q}' - 2\boldsymbol{\omega}'), \tag{13}$$

$$\left[\frac{\partial T'}{\partial t} + w\frac{\Delta T}{d} f(z) \right] = \chi \nabla^2 T' + \frac{\beta}{\rho_0 C_v} \left[(\nabla \times \boldsymbol{\omega}').\left(\frac{\Delta T}{d} f(z)\right) \hat{k} \right], \tag{14}$$

$$\rho' = -\rho_0 \alpha_t T' + \rho_0 \alpha_s C', \tag{15}$$

$$\left[\frac{\partial C'}{\partial t} + (w\frac{\Delta C}{d} g(z) \right] = \chi_s \nabla^2 C'. \tag{16}$$

The perturbation Eqs. (11)–(16) are non-dimensionalized using the following definitions:

$$(x^*, y^*, z*) = \left(\frac{x}{d}, \frac{y}{d}, \frac{z}{d}\right), \nabla^{*2} = d^2\nabla^2, \mathbf{q}^* = \frac{\mathbf{q}}{\frac{k}{d}}, t^* = \frac{t}{\frac{d^2}{\chi}}, \tag{17}$$

$$p^* = \frac{p}{p_0}, T^* = \frac{T}{\Delta T}, C^* = \frac{C}{\Delta C}, W^* = \frac{W}{\frac{\chi}{d}}. \tag{18}$$

Using Eq. (15) in Eq. (12), curl is applied twice on the following equation. Curl is applied once on Eq. (13) as well and the derived two equations are then non-dimensionalized along with Eqs. (14) and (16). After ignoring the asterisks, the following equations are obtained:

$$\frac{1}{Pr}\frac{\partial}{\partial x}(\nabla^2 W) = R\nabla_1^2 T - R_s\nabla_1^2 C + (1+N_1)\nabla^4 W + N_1\nabla^2\Omega_z, \quad (19)$$

$$\frac{N_2}{Pr}\frac{\partial\Omega_z}{\partial t} = N_3\nabla^2\Omega_z - N_1\nabla_2 W - 2N_1\Omega_z, \quad (20)$$

$$\frac{\partial T}{\partial t} = \nabla^2 T + (-W + N_5\Omega_z)f(z), \quad (21)$$

$$\frac{\partial C}{\partial t} = \tau\nabla^2 C - Wg(z), \quad (22)$$

where Rayleigh Number $\left[R = \frac{\rho_0\alpha g\Delta T d^3}{(\eta+\zeta)\chi}\right]$, solutal Rayleigh Number $\left[R_s = \frac{\rho_0\alpha_s g\Delta C d^3}{(\eta+\zeta)\chi}\right]$, coupling Parameter $\left[N_1 = \frac{\zeta}{\zeta+\eta}\right]$, couple stress parameter $\left[N_3 = \frac{\eta'}{(\zeta+\eta)d^2}\right]$, micropolar heat conduction parameter $\left[N_5 = \frac{\beta}{\rho_0 C_v d^2}\right]$, and ratio of diffusivity $\left[\Gamma = \frac{\chi_s}{\chi}\right]$ are the non-dimensional parameters used.

A normal mode solution for the stationary convection is obtained as the infinitesimal perturbations W, Ω_z, T and C are assumed to be periodic waves [8]. The solution is represented as

$$[W, \Omega_z, T, C] = [W(z).e^{i(lx+my)}, G(z).e^{i(lx+my)}, T(z).e^{i(lx+my)}, C(z).e^{i(lx+my)}]. \quad (23)$$

Here, the wave number a has horizontal components l and m. Equation (23) is substituted in Eqs. (19)–(22) to obtain

$$-Ra_2 T + R_s a^2 C + (1+N_1)(D^2 - a^2)^2 W + N_1(D^2 - a^2)^2 G = 0, \quad (24)$$

$$\left[2N_1 - N_3(D^2 - a^2)\right]G + N_1(D^2 - a^2)^2 W = 0, \quad (25)$$

$$(D^2 - a^2)T + (-W + N_5 G)f(z) = 0, \quad (26)$$

$$\left[\tau(D^2 - a^2)\right]C - Wg(z) = 0, \quad (27)$$

where $a^2 = l^2 + m^2$.

Applying the Galerkin procedure to Eqs. (24)–(27), we obtain general results on the eigenvalue for different temperature gradients under the given boundary conditions by considering trial functions for velocity $W(z, t)$, microrotation $G(z, t)$, and temperature $T(z, t)$, concentration perturbations $C(z, t)$.

$$W(z, t) = \sum A_i(t)W_i(z), \quad G(z, t) = \sum E_i(t)G_i(z),$$
$$T(z, t) = \sum B_i(t)T_i(z), \quad C(z, t) = \sum F_i(t)C_i(z),$$

where $A_i(t), E_i(t), B_i(t)$, and $F_i(t)$ are constant functions and $W_i(z), G_i(z), T_i(z)$, and $C_i(z)$ are polynomials in z, that generally satisfy the given boundary conditions.

Now taking $i = j = 1$, Eqs. (24), (25), (26), and (27) are multiplied by W, G, T, and C, respectively. The resulting equation is integrated by parts with respect to

z from 0 to 1. The equation for the Rayleigh number is generated by substituting $W = AW_1; G = EG_1; T = BT_1; C = FC_1$, where A, B, E, and F are constants and W_1, G_1, T_1, and C_1 are the trial functions:

$$R = \left[\frac{X_1 X_3 L_7}{a^2 L_1(\langle W_1 T_1 f(z) \rangle X_1 - N_1 N_5 \langle T_1 G_1 f(z) \rangle L_5)} \right], \quad (28)$$

where

$$X_1 = N_3 L_2 - 2N_1 L_3, \quad X_3 = \frac{R_s a^2 L_8 \langle W_1 C_1 \rangle}{-\tau L_{10}} + L_{14}$$

$$L_1 = \langle W_1 T_1 \rangle, \quad L_2 = \langle G_1(D^2 - a^2)G_1 \rangle, \quad L_3 = \langle G_1^2 \rangle, \quad L_4 = \langle T_1 G_1 \rangle,$$

$$L_5 = \langle G_1(D^2 - a^2)W_1 \rangle, \quad L_6 = \langle T_1^2 \rangle, \quad L_7 = \langle T_1(D^2 - a^2)T_1 \rangle,$$

$$L_8 = \langle W_1 C_1 \rangle, \quad L_9 = \langle C_1^2 \rangle, \quad L_{10} = \langle C_1(D^2 - a^2)C_1 \rangle,$$

$$L_{11} = \langle W_1(D^2 - a^2)^2 W_1 \rangle, \quad L_{12} = \langle W_1(D^2 - a^2)W_1 \rangle, \quad L_{13} = \langle W_1(D^2 - a^2)G_1 \rangle,$$

$$L_{14} = (1 + N_1)L_{11} + \frac{N_1^2 L_5 L_{13}}{X_1}, \quad L_{15} = \langle W_1 T_1 f(z) \rangle, \quad L_{16} = \langle T_1 G_1 f(z) \rangle.$$

Here, integral with respect to z under the limits $z = 0$ and $z = 1$ (for calculation purpose, we have taken the distance between the plates as $d = 1$) is denoted by $\langle \ldots \rangle$. The value of the concentration gradient $g(z)$ is taken as 1 in Eq. (27) to examine the effect of non-uniform temperature profiles.

The combinations of boundary conditions considered in this problem are Free–Free Isothermal-Permeable No-Spin condition, Rigid–Free Isothermal-Permeable No-Spin condition, and Rigid–Rigid Isothermal-Permeable No-Spin condition. The critical Rayleigh number is subjected to the three boundary conditions and the value of the trial functions that satisfy them are taken as $W_1 = 3z - 2z^2 + z^4, 4z - 6z^3 + 3z^4$ and $5z^4 - 6z^3 - z^2$, respectively, and $G_1 = T_1 = C_1 = 2z(z - 1)$.

5 Results and Discussion

5.1 Effects of Non-uniform Temperature Gradient Profiles

The effects of one uniform and three non-uniform temperature gradient profiles on the onset of salt finger convection in a micropolar liquid are examined in this paper. The values of these profiles are discussed in Table 1. To analyze the effect of the temperature gradient, the value of the concentration gradient $g(z)$ is taken as 1 and the following observations are made:
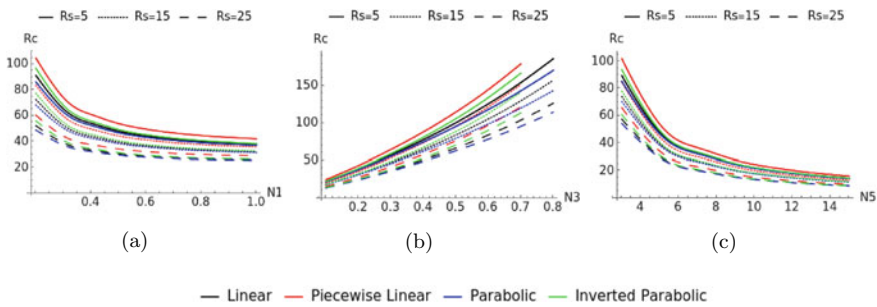
For Free–Free and Rigid–Free boundary condition,
$$R_{CM3} < R_{CM1} < R_{CM4} < R_{CM2}.$$

For Rigid–Rigid boundary condition, $R_{CM4} < R_{CM1} < R_{CM2} < R_{CM3}$.

Figures 2 and 3 represents the graphs of critical Rayleigh number R_C plotted against micropolar liquid parameters N_1, N_3, and N_5 taken one at a time while keeping the other two fixed for various solutal Rayleigh number R_S and ratio of diffusivity under free–free and rigid–rigid boundary conditions, respectively. The graphs are obtained for the non-uniform temperature profiles mentioned in Table 1.

Under free–free boundary conditions, the inverted parabolic function appears to be the temperature profile that destabilizes the system considerably compared to the other profiles and the piecewise function profile comparatively stabilizes the system. (The same effect can be observed for rigid–free boundary conditions), whereas, for rigid–rigid boundary conditions, the parabolic function is the temperature profile that destabilizes the system the most, and the inverted parabolic function profile comparatively stabilizes the system.

Fig. 2 **a** R_c is plotted against N_1 by fixing $N_3 = 0.1$, $N_5 = 5$, and $\tau = 0.2$, **b** R_c is plotted against N_3 by fixing $N_1 = 0.5$, $N_5 = 10$, and $\tau = 0.2$, **c** R_c is plotted against N_5 by fixing $N_1 = 0.5$, $N_3 = 0.1$, and $\tau = 0.2$ for free–free boundary condition
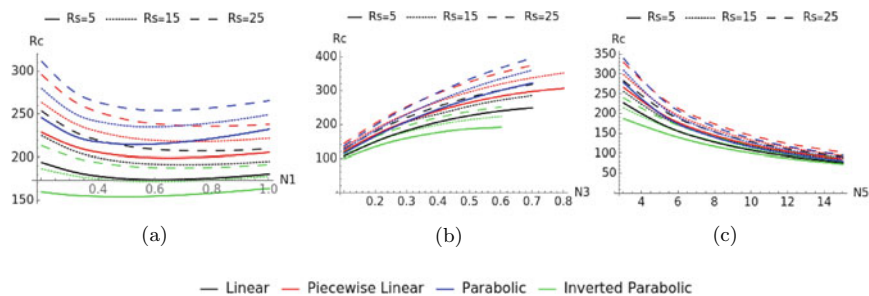
Fig. 3 **a** R_c is plotted against N_1 by fixing $N_3 = 0.1$, $N_5 = 5$, and $\tau = 0.2$, **b** R_c is plotted against N_3 by fixing $N_1 = 0.5$, $N_5 = 10$, and $\tau = 0.2$, **c** R_c is plotted against N_5 by fixing $N_1 = 0.5$, $N_3 = 0.1$, and $\tau = 0.2$ for rigid–rigid boundary condition

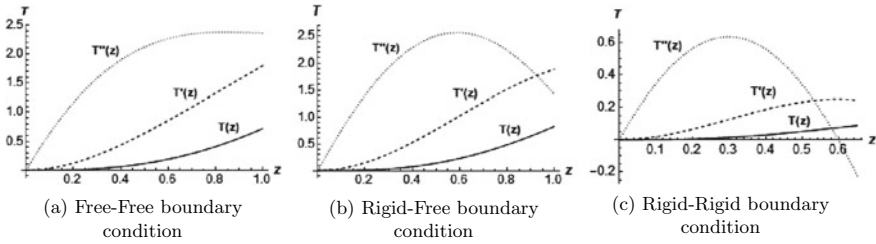| (a) Free-Free boundary condition | (b) Rigid-Free boundary condition | (c) Rigid-Rigid boundary condition |

Fig. 4 Phase of temperature flow

5.2 *Phase of Temperature Flow*

The graphs for the phase of temperature flow are plotted for free–free, rigid–free, and rigid–rigid boundary conditions (Fig. 4a, b, c). They are obtained by solving the conservation of energy equation (temperature equation) numerically for different cases as mentioned. The x-axis and the y-axis represent the distance between the parallel plates and the amount of the temperature supplied from above into the system, respectively. These plots are basically the graphical representation of the solution of $T(z)$ and its first and second derivatives. From Fig. 4a, b, c, the following observations can be made: (i) Temperature is more at $z = 1$ (upper plate) and decreases gradually as we move towards $z = 0$ (lower plate). This is because the temperature is supplied from above and the diffusion rate will be higher or faster near the upper plate. Later, it slows down as it comes in contact with the colder molecules in the system (it is also because heat diffuses much faster than solute in the beginning). (ii) The phase of temperature flow of $T(z)$ is lesser than its derivatives. (iii) For rigid–rigid boundary conditions, the temperature flow effect will be seen only towards the center of the system and near the upper plate. This is mainly because the plates are rigid, hence more amount of temperature is required for the onset of convection.

6 Conclusion

- The inverted parabolic function appears to be the temperature profile that destabilizes the system in free–free and rigid–free boundary conditions.
- The piecewise function profile comparatively stabilizes the system in free–free and rigid–free boundary conditions.
- The parabolic function is the temperature profile that destabilizes the system the most in rigid–rigid boundary conditions.
- The inverted parabolic function profile comparatively stabilizes the system in rigid–rigid boundary conditions.
- The Micropolar parameters N_1 and N_5 destabilize the system with respect to R_c in all the boundary conditions.

- The Micropolar parameters N_3 stabilize the system with respect to R_c in all the boundary conditions.
- The phase of temperature flow will explain the variation of the temperature between the parallel plate boundary (i.e., at $z = 0$ and at $z = d$). Finally, it is observed that the temperature distribution is more at the upper plate boundary and this is due to the nature of salt fingers (as shown in the schematic diagram).

References

1. Stern ME (1960) The 'Salt-Fountain' and thermohaline convection. Tellus 12(2): 172–175
2. Jevons WS (1858) On clouds; their various forms, and protruding causes. Syd Mag Sci Art 1:163–176
3. Ekman VW (1906) "On dead water", Scientific results of the Norwegian North Polar. Expedition 5:1–152
4. Stommel H, Arons AB, Blanchard D (1956) An oceanographical curiosity: the perpetual salt fountain. Deep Sea Res 3(2):152–153. https://doi.org/10.1016/0146-6313(56)90095-8
5. Eringen AC (1965) Theory of micropolar fluids
6. Lukaszewicz G (1999) Micropolar fluids-theory and applications. Birkhauser, Boston
7. Pranesh S, Narayanappa A (2012) Effect of non-uniform basic concentration gradient on the onset of double-diffusive convection in micropolar fluid. Appl Math 3(5):417–424. https://doi.org/10.4236/am.2012.35064
8. Chandrasekhar S (1981) Hydrodynamic and hydromagnetic stability. Dover Publications, New York